




## Article

# Long-Term Wind and Air Temperature Patterns in the Southeastern Region of Iran through Model Simulation and Ground Observations

Nasim Hossein Hamzeh <sup>1</sup>, Abbas Ranjbar Saadat Abadi <sup>2,\*</sup>, Khan Alam <sup>3</sup>, Karim Abdulkhakimovich Shukurov <sup>4</sup> and Christian Opp <sup>5,\*</sup>

<sup>1</sup> Department Meteorology, Air and Climate Technology Company (ACTC), Tehran 15996-16313, Iran; nasim\_hh@yahoo.com

<sup>2</sup> Meteorology Department, Atmospheric Science and Meteorological Research Center (ASMERC), Tehran 14977-16385, Iran

<sup>3</sup> Department of Physics, University of Peshawar, Peshawar 25120, Pakistan; khanalam@uop.edu.pk

<sup>4</sup> A.M. Obukhov Institute of Atmospheric Physics, Russian Academy of Sciences, Moscow 119017, Russia; karim.shukurov@ifaran.ru

<sup>5</sup> Department of Geography, Philipps-Universität Marburg, 35037 Marburg, Germany

\* Correspondence: a-ranjbar@irimo.ir (A.R.S.A.); opp@staff.uni-marburg.de (C.O.)

**Abstract:** Dust storms are one of the important natural hazards that affect the lives of inhabitants all around the world, especially in North Africa and the Middle East. In this study, wind speed, wind direction, and air temperature patterns are investigated in one of the dustiest cities in Sistan Basin, Zahedan City, located in southeast Iran, over a 17-year period (2004–2020) using a WRF model and ground observation data. The city is located near a dust source and is mostly affected by local dust storms. The World Meteorology Organization (WMO) dust-related codes show that the city was affected by local dust, with 52 percent of the total dust events occurring during the period (2004–2021). The city's weather station reported that 17.5% and 43% were the minimum and maximum dusty days, respectively, during 2004–2021. The summer and July were considered the dustiest season and month in the city. Since air temperature, wind speed, and wind direction are important factors in dust rising and propagation, these meteorological factors were simulated using the Weather Research and Forecasting (WRF) model for the Zahedan weather station. The WRF model's output was found to be highly correlated with the station data; however, the WRF simulation mostly overestimated when compared with station data during the study period (2004–2020). The model had a reasonable performance in wind class frequency distribution at the station, demonstrating that 42.6% of the wind was between 0.5 and 2, which is in good agreement with the station data (42% in the range of 0.5–2). So, the WRF model effectively simulated the wind class frequency distribution and the wind direction at Zahedan station, despite overestimating the wind speed as well as minimum, maximum, and average air temperatures during the 17-year period.

**Keywords:** wind speed and wind direction; air temperature; dust events; WRF model; Zahedan



**Citation:** Hamzeh, N.H.; Abadi, A.R.S.; Alam, K.; Shukurov, K.A.; Opp, C. Long-Term Wind and Air Temperature Patterns in the Southeastern Region of Iran through Model Simulation and Ground Observations. *Atmosphere* **2024**, *15*, 993. <https://doi.org/10.3390/atmos15080993>

Academic Editor: Avelino Eduardo Saez

Received: 20 May 2024

Revised: 9 August 2024

Accepted: 12 August 2024

Published: 19 August 2024



**Copyright:** © 2024 by the authors. Licensee MDPI, Basel, Switzerland. This article is an open access article distributed under the terms and conditions of the Creative Commons Attribution (CC BY) license (<https://creativecommons.org/licenses/by/4.0/>).

## 1. Introduction

Dust storms are severe environmental disasters, every year affecting millions of human lives and properties all around the world [1,2]. The Middle East is the second dust source in the world after North Africa, contributing 15–20% to dust load of the atmosphere in the world [3,4]. Although most dust storms originate from desert areas, recently dried lake beds turn out to be the second largest dust source, especially at local and regional scales [5–8]. Iran is located in the Middle East and is greatly affected mostly by external and internal dust sources [9–12]. Although Iranian territory is affected by different dust sources, the main external dust source is the Mesopotamian Plain in Iraq and also deserts of Iraq and Syria [13]. Among internal dust sources, the Al-Howizeh/Al-Azim marshes

in the southwest of Iran and the Sistan Basin in southeast of Iran were identified as the main sand and dust storm (SDS) source areas in the country [14–17]. Unfortunately, the Al-Howizeh/Al-Azim dust sources are still expanding [13] and the region is suffering from rapid land degradation [18,19]. Also, the Sistan Basin is affected due to wind erosion and rapid soil degradation [20,21]. The Levar wind (which lasts for 120 days) has a direct impact on dust rising and dust transportation in the Sistan Basin [22,23].

In the process of dust particle emission, surface conditions are crucial [24] among the other meteorological factors, like wind speed and wind direction [8,25], relative humidity [26], air temperature [27], and surface pressure [28,29]. Also, soil moisture [30], vegetation cover [9,31], land use [32], slope [33], and topography [34] are some important surface conditions that contribute significantly to dust particle emission [5]. Furthermore, climatic factors, such as increasing air and surface temperatures, decreasing precipitation, and long droughts, directly favor directly an increase in dust event frequency in the Middle East [9].

Among the meteorological factors, wind speed and wind direction have an important and direct role in the rising of dust from a dust source as well as in the transport and propagation in (and from) the affected area [6,7,35–38]. Severe wind causes dust particles to rise from the dust hotspot, while wind direction determines the area affected by the dust storm [8]. Many experiments have been carried out with wind tunnels to investigate wind speed threshold to cause dust particles to rise, depending on different types of soil texture [36–40]. Furthermore, some models, such as The Hybrid Single-Particle Lagrangian Integrated Trajectory (HYSPPLIT) model, allow the computation of backward or forward air parcel trajectories to determine either potential sources of dust particles or their probable paths of propagation [5,6,39–43]. Thus, wind speed and wind direction are important parameters that can be used for investigating the formation and propagation of dust storms [44–47].

The southeastern region of Iran, encompassing the Lut desert valley and the dry lake of Jaz Morian, is characterized by the presence of a prevalent low-level northerly jet [48–50]. This jet is the result of various factors operating at different scales and can lead to the generation and transport of dust while passing through these arid regions [48]. The formation of this low-level jet is influenced by complex processes; as it moves through the Lut desert valley and the dry lake of Jaz Morian, it can resuspend and transport dust, thus limiting visibility and degrading electromagnetic and optical propagation, especially when reaching the Gulf of Oman [49,50]. Furthermore, a severe local wind, called the Levar wind or 120-day wind, is frequently blown to this area, so in the appropriate situation, dust particles rise and propagate in this area [23,25]. The wind intensifies while passing through the tunnels in the Hindukush mountains. Also, vast parts of southeast Iran receive less than 40 mm of annual rainfall, which is another important factor for soil vulnerability to dust rising. Thus, the arid climate of this region plays a central role in dust rising [16,25].

In the Sistan Basin, the dried-up areas of Lake Hamon recently became a significant dust source, becoming the most active dust source inside Iran [16]. Additionally, the studied region is situated in close proximity to two major Iranian deserts: Dasht-e-Lut and Dasht-e-Kavir (Great Salt Desert). Furthermore, this area is affected by one of the strongest winds in Iran, called the Levar wind [35]. These factors resulted in dust storms becoming a dominant phenomenon in the region [16,25]. Furthermore, severe soil erosion is one of the important consequences of dust rising, and dust storms can also lead to extensive environmental consequences for the local residents [16,51]. The presence of abundant dust sources, the proximity to large deserts, and the prevalence of high winds in the area all contributed to the prominence of dust storms as a major issue in this region and the surrounding area [16,24,25]. Visual observations from meteorological stations across Turkmenistan, Iran, Afghanistan, and Pakistan have revealed that the highest frequency of dust storms is observed in the Sistan Basin and the surrounding deserts of southern Afghanistan [52,53]. Additionally, a long-term study in the Sistan Basin found a statistically

significant increasing trend in PM10 concentrations, which is driven by a rise in the speed of the local Levar wind, particularly after 2017 [54].

In this study, the number of WMO dust-related codes (06, 07, 08, 09, 30–35, and 98) was investigated through the data of the Zahedan weather station measured in 2000–2021. Also, the annual, seasonal, and monthly numbers of dust events were investigated for the determination of high and low dust frequency in 2000–2021. In the next step, the WRF model was run for 17 years (2004–2020) for simulation of 10 m wind speed and wind direction as well as minimum, average, and maximum air temperatures at the station during the same period. Furthermore, the simulated meteorological parameters were compared with station data at the Zahedan station. While previous studies have emphasized the significance of the Levar wind in driving dust mobilization in the Sistan Basin [55–57], the current work aims to assess the capability of the WRF model in simulating wind speed, wind direction, and air temperature at the Zahedan station. This investigation aims to elucidate the role of wind and air temperature in one of the critical dust source regions in southeastern Iran, as well as to evaluate the performance of WRF model simulations over areas prone to dust events.

## 2. Study Area

Zahedan City (29.32° N, 60.52° E, 1384 m asl) in southeast Iran is near the Iranian borders with Afghanistan and Pakistan (Figure 1). The city is located in the south of the Sistan Basin, so it is mostly affected by dust storms mainly originating from the basin, especially in the summer season [58]. The Levar (or 120-day) wind dominates in this area, so the wind has crucial role in rising dust in the Sistan Basin [25,58]. The local wind is mostly dominant for four months (mid-May to mid-September) but lasts for more than 120 days [16,25]. The city is the center of the Sistan and the Blochestan Province, with a population of more than 800 thousand people [59]. The climate of the city is semi-arid to arid and the high and low air temperatures of the city are observed in summer (around 33 °C) and winter (between 10 and 13 °C), respectively.

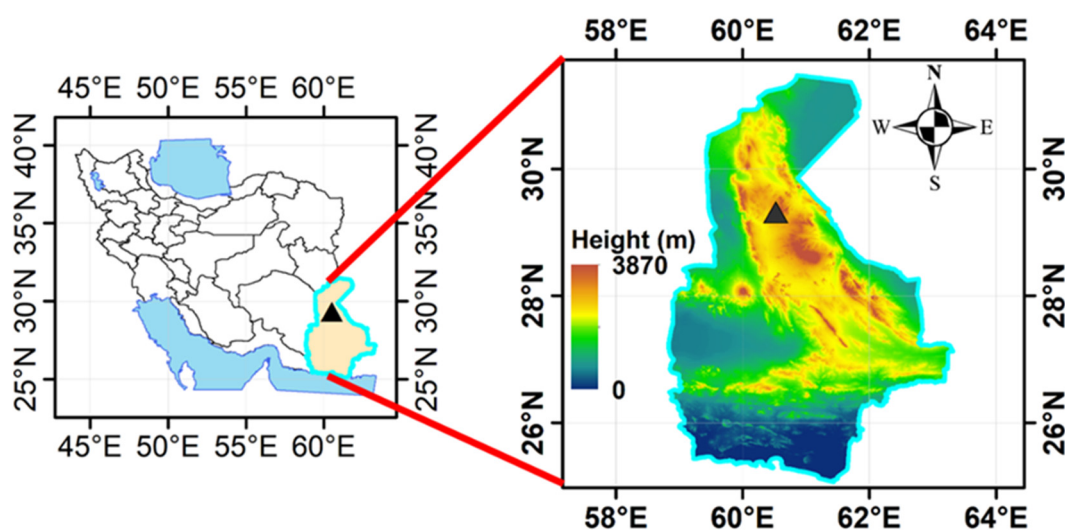


**Figure 1.** Topography of the Sistan Basin (southeast Iran) with the synoptic weather stations of Zahedan City (marked with black triangle).

The Zahedan weather synoptic station is a manual weather station in Iran that meets WMO standards. However, the measurement of horizontal visibility is taken visually and approximately, which can introduce errors. Additionally, sensor calibration and environmental factors can affect the accuracy of temperature measurements. Sensor accuracy, local turbulence, local terrain, and nearby obstacles can influence wind data.

Simulations from numerical weather forecasting models can also be associated with uncertainties due to the following reasons. (i) Model physics: Limitations in the representa-

tion of physical processes can introduce uncertainties in the model outputs. (ii) Boundary and initial conditions: Errors in the input data can propagate through the model and can affect the simulated temperature and wind field. (iii) Topographic and land use representation: Accurate representation of complex terrain and land use characteristics can be challenging.

These inherent uncertainties must be considered when comparing point-scale observational data and model-generated grid-scale data. It is crucial to understand the limitations and uncertainties associated with both the measured data and the WRF model results to draw reliable conclusions. Some differences between the observational quantities and the model simulation should be expected and accepted.

### 3. Dataset and Methodology

The data used in this study were obtained from the meteorological synoptic station in Zahedan and the output of the Weather Research and Forecasting (WRF) model. The observational data were recorded at 3 h intervals and included air temperature, wind field, horizontal visibility, current weather, and the type of phenomenon, including codes related to sandstorms. The WRF model output included wind field and air temperature data at 1 h time steps and a horizontal resolution of approximately 5 km.

The study period was analyzed using weather station reports from Zahedan, which provided information on dust-related codes, air temperature, wind speed, and wind direction. Additionally, ECMWF ERA-Interim reanalysis data with a spatial resolution of  $0.75^\circ \times 0.75^\circ$ , a temporal resolution of 6 h, and up to 60 vertical levels were used as initial and boundary conditions for the WRF model [60–64]. Numerical weather forecasting models like WRF can be used to fill data gaps in areas without measurement stations, such as deserts and regions with complex topography. However, both the measured data and the WRF model results have associated uncertainties that should be considered when analyzing the potential sources of error and their implications for the study's observations.

#### 3.1. Meteorology Dust-Related Data

The annual, seasonal, and monthly frequencies of dust events are analyzed using the data obtained at Zahedan station during the period (2000–2021). In this study, the WMO dust-related codes 06, 07, 30 to 35, and 98 are used for the study duration in Zahedan station. The codes were reported 8 times a day i.e., every 3 h. In this study, a dusty day is a day with at least one dust-related code detected among all 8 reports during the whole day.

Dust-related code 06 indicates widespread dust that is not due to the wind at or near the station, i.e., the code is related to non-local dust. The criteria for this code include low wind speed. Code 07 is related to dust or sand raised by wind at or near the station, reducing the horizontal visibility. The criteria for this code include a wind speed of 7 m/s or more, and there is no limit to the horizontal visibility reduced due to the presence of dust or sand, so it indicates local dust events (codes 5, 6, 9), while dust codes 30–35 and 98 happened very rarely over Zahedan station. Codes 30–35 indicate a dust storm or sandstorm within sight at the time of observation or during the preceding hour. The criteria for these codes include a wind speed of 30 knots (approximately 15 m/s) or more, and the horizontal visibility is reduced to less than 1 km due to the presence of a dust or sandstorm. These codes indicate the intensity of the dust events, with the lower codes (30–32) representing weaker events and the higher codes (33–35) representing more intense dust storms [65]. Code 98 indicates the presence of a thunderstorm and a dust or sandstorm.

It is important to note that the criteria for these codes consider the combination of wind speed, horizontal visibility, and the presence and intensity of the dust or sand being raised. These factors collectively determine the appropriate code to be assigned for a particular dust event.

### 3.2. Air Temperature, Wind Speed, and Wind Direction Data

The meteorological parameters (air temperature, wind speed, and wind direction) were measured at Zahedan station during the period (2005–2021). The data were reported every 3 h (8 times) during a day. In this study, the meteorological data and WRF simulation outputs are used for comparison purposes.

### 3.3. WRF Model

The WRF model is a regional model for numerical weather predictions and meteorological research [66–71]. In this study, the WRF model (version 3.9) was utilized to simulate wind speed, wind direction, and air temperature across Iran during the period (2004–2020). The resulting simulated data will be used to prepare a comprehensive wind atlas of Iran, as reported in a separate study [35].

To optimize the model's performance for the complex terrain of Iran, the WRF model was implemented with two-way nested domains. The first, larger domain covered the Middle East region at a horizontal resolution of 15 km, while the second, higher-resolution domain focused on Iran at 5 km (Figure 2). This nesting approach allowed the model to better resolve the intricate topographic features of the study area. Additionally, the model was configured with 39 vertical levels, extending from the surface up to the 100 hPa pressure level. The first six vertical levels were positioned at approximately 12, 35, 65, 100, 140, and 200 m above the ground, ensuring a detailed representation of the atmospheric boundary layer.

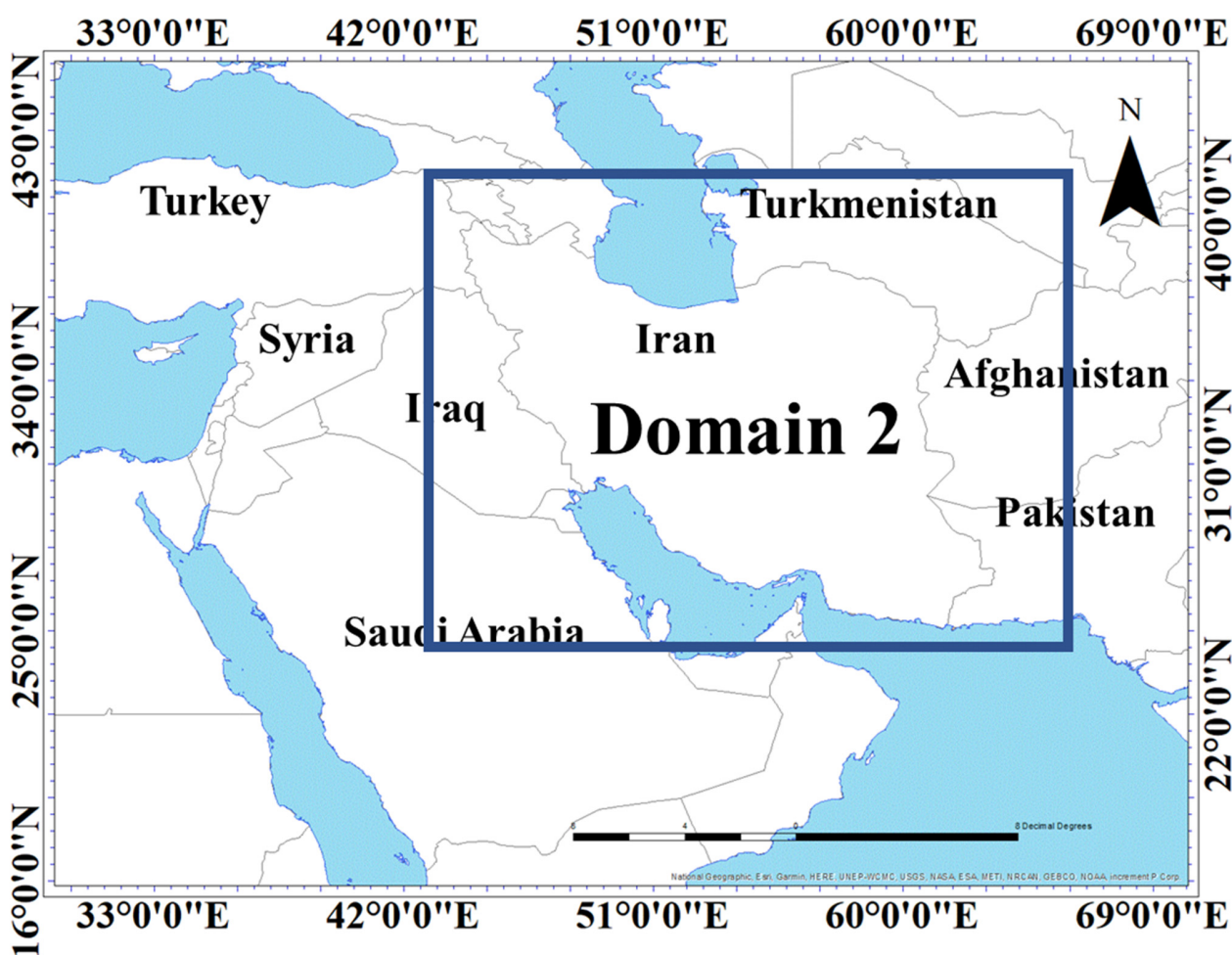


**Figure 2.** The two domains of the WRF model simulations over the Middle East whole figure (domain1) and Iran (domain2).

The physical parameterization schemes used in the WRF model included:

- Microphysics: Lin et al. scheme [72];
- Longwave Radiation: RRTM scheme [73];
- Shortwave Radiation: Dudhia scheme [74];
- Land Surface: Noah Land Surface Model [75];
- Planetary Boundary Layer: ACM2 [76].

Initially, the WRF model underwent simulations using five distinct planetary boundary layer (PBL) schemes, namely YSU, MYJ, MYNN2.5, QNSE, and ACM2. Subsequently, after a thorough evaluation, the ACM2 boundary layer scheme emerged as the most effective scheme among the options considered. The outputs from the higher-resolution (5 km) domain were compared with observational data from synoptic stations, upper-air soundings, and meteorological towers. The results of this comparative analysis demonstrated that the ACM2 boundary layer scheme provided the most accurate representation of the wind and temperature patterns in the study region, leading to its selection for the final simulations.

#### 4. Results and Discussion

##### 4.1. Investigation of Ground-Based Dust Reports

Figure 3 shows the percentages of the WMO codes related to dust including 06, 07, 08, 09, 30–35, and 98, at Zahedan meteorological station during the period (2004–2021). Codes 08, 09, 30–35, and 98 were rarely reported at the station and they contribute only 4% of all reported dust codes, while 52% of all reported dust codes were related to code 07 (local dust), and 44% were related to dust code 06 (non-local dust). Despite the fact that the city of Zahedan is located close to dust sources, it is also affected by non-local dust, with a lower percentage of dust transported from long ranges. The Levar wind is mostly dominant in the stations located in the Sistan Basin, so a high percentage of local dust is not far from expected [6]. The situation is totally different in west and southwest Iran and the area mostly affected by dust storms originating from the Mesopotamian Plain and the deserts in Iraq and Syria [71,77–82].

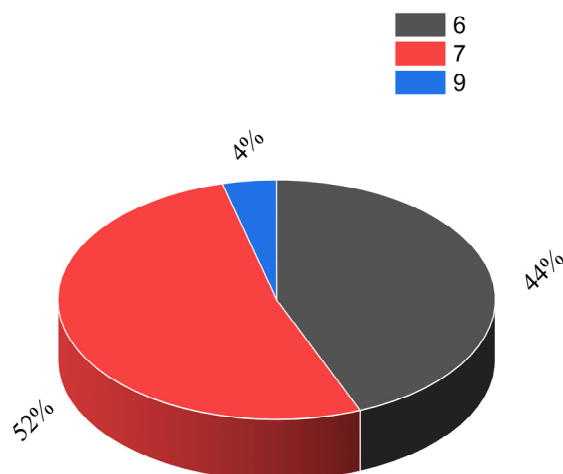


**Figure 3.** Percentage of WMO dust-related codes from the data of Zahedan meteorological station obtained in 2004–2021.

Figure 4a shows the annual number of dust events in the period from 2004 to 2021. The minimum number of dusty days was reported in 2020 (64 days), while the maximum (157 days) was observed in 2008. This means that the station is affected by dust storms for, at minimum, 17.5% of a year, and a maximum of 43% of a year. The pattern of highest dust duration is totally different compared to west, SW, and NW Iran [5–9]. In west and southwest Iran, the highest dust frequencies happened from 2008 to 2013, in agreement

with a long drought in the Iraqi Plains [9,66–69], and the same high dust frequency was reported in Kuwait, Saudi Arabia, and a large part of the Arabian Peninsula [79–82].

Figure 4b shows the number of dusty days in different months at Zahedan in 2004–2021. The highest value of monthly dust frequency was reported in July (301 days) followed by August (225 days). As expected, the highest dust frequency was reported in coincidence with the Levant wind duration from mid-May to mid-September. Also, the lowest dust frequency is found in November (53 days in the whole study duration).

Figure 4c shows the number of dusty days in different seasons at Zahedan in 2004–2021. The highest value of seasonal dust frequency was reported in the summer (660 days) followed by spring (509 days). As expected, the highest dust frequency was related to warm seasons. In contrast, the lowest dust frequency was related to autumn (211 days) during the period (2004–2021). The same pattern was observed in southwest Iran, where the highest dust frequencies were reported in the summer and then in the spring [9,76–80]. So, the highest dust frequencies happened in the warm part of the year at Zahedan station, in agreement with northwest [5,81–84] and southwest Iran [9,85–88].

To investigate the continuity of dust occurrences on each dusty day, the number of three-hour occurrences on dusty days were calculated (Figure 4d). The analysis revealed that between 2004 and 2008, the persistence of dust was notably higher than the period average. In contrast, from 2009 to 2021, the dust persistence on dusty days decreased below the period average, reaching its lowest values in 2010 and 2011. The occurrence of dust in an area is influenced by two primary factors: the characteristics of the earth's surface, such as soil type, moisture levels, and vegetation, and atmospheric conditions, including wind speed [16]. It is plausible that during the initial period (2004–2008), the region experienced prolonged droughts, coupled with consistent high-speed winds, contributing to increased dust presence. Conversely, in the later period (2009–2021), being a desert region, the potential for dust production remained high. The observed decline in dust persistence during this period is likely attributed to shifts in large-scale atmospheric patterns, which play a crucial role in dust generation.

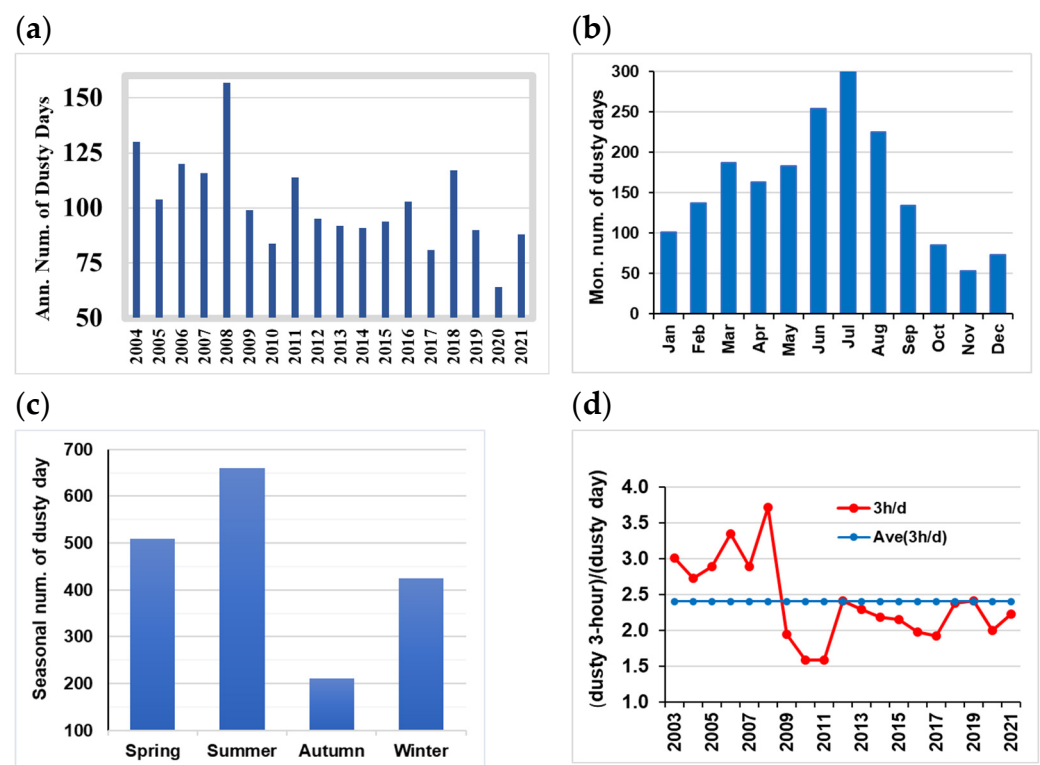


**Figure 4.** (a) Annual, (b) monthly, and (c) seasonal number of dust events and (d) number of 3 h dust events on dusty days at Zahedan station from 2004 to 2021.

4.2. WRF Model Simulations

4.2.1. WRF Model Simulations of Air Temperature

Figure 5 shows the annual mean, minimum, and maximum of the WRF model simulations and the measured data of air temperature at Zahedan station from 2004 to 2020. Figure 5a shows that the WRF model underestimated the mean annual air temperature during the study period. The highest discrepancies are related to 2004 with 3.9 m/s, and the lowest is related to 2008 with 2.6 m/s. However, the correlation coefficient between the WRF model outputs and the station data is high, at 0.82. The figure indicates that the fluctuation patterns of both observed and simulated results are in good agreement with each other. Figure 5b shows that the WRF model underestimated minimum annual air temperature in 2004–2020. The highest discrepancy is related to 2012 with 4.5 °C and the lowest is related to 2004 with 0.2 °C. The model mostly underestimated minimum temperature in the study period and overestimated it in some years (see values in 2008, 2011, 2014, and 2017). Despite this, the correlation coefficient between WRF outputs and the station data was reasonable (0.59). Figure 5c indicates that the WRF model underestimated maximum annual air temperatures in 2004–2020. The highest discrepancy is related to 2004 with 4.3 °C, and the lowest is related to 2010 with 1.4 °C. Also, the correlation coefficient between WRF outputs and the station data was 0.59, with a similar fluctuation pattern. The synoptic data from Zahedan station during the study period of 2004–2020 have less than 0.2% incomplete or missing data, which does not significantly affect the monthly and annual data. The large differences between the model and observed data in certain years cannot be solely attributed to the incompleteness of the data. These differences can be attributed to variations in the prevailing weather conditions in different years, such as droughts, atmospheric front activities, or other meteorological factors [78].

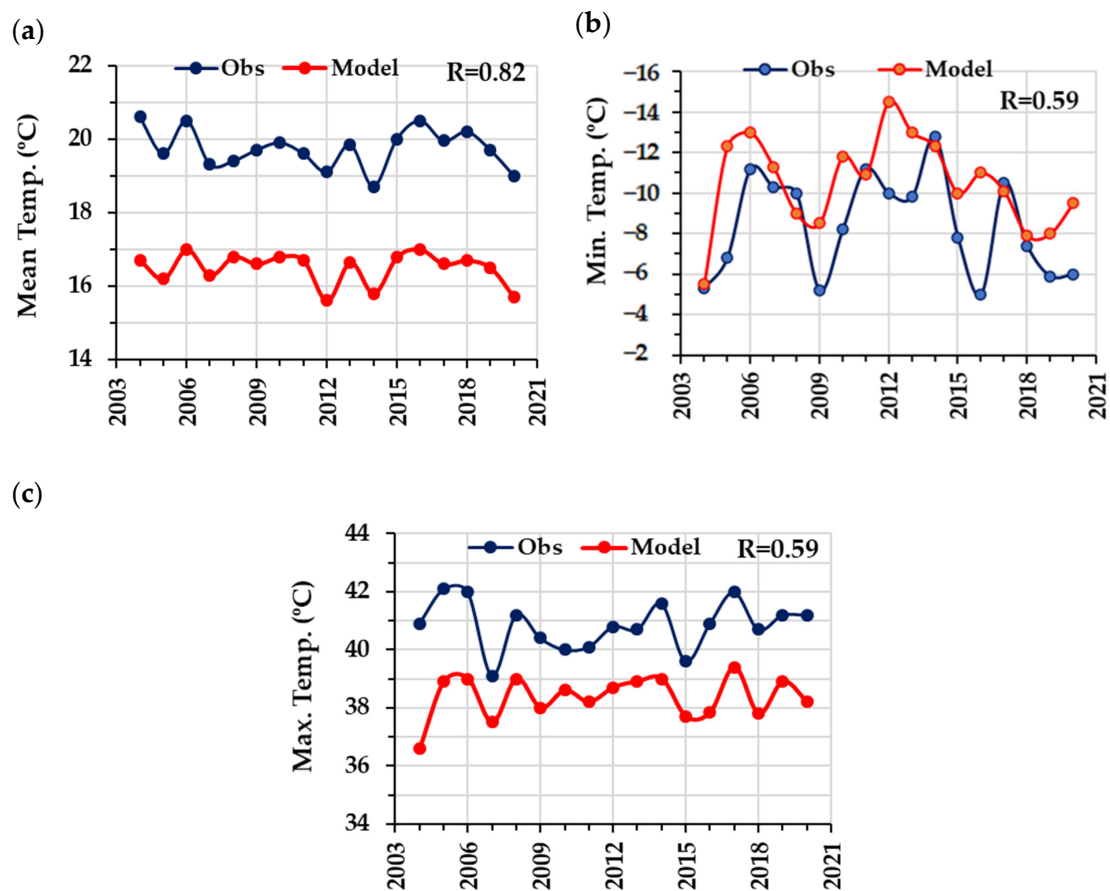


Figure 5. (a) Annual mean, (b) minimum, and (c) maximum air temperature during 2004–2020 at Zahedan station by WRF simulation (red line) and by measured data (black line).



When comparing the differences between the simulated and observed temperatures, it is evident that the changes in the observational data and the simulated data show good agreement for maximum and average temperatures. The differences between the two datasets are typically around 2 °C to 3 °C in most years, suggesting the presence of systematic errors in the model simulations, which can be reduced by applying post-processing techniques.

Another potential source of error is the difference between the method of recording the minimum and maximum temperatures in manual synoptic stations and the data extracted from hourly model simulations. If the maximum and minimum temperatures occurred within a one-hour interval, this temporal mismatch may not be accurately captured in the model data, but it is reflected in the observational data.

Furthermore, the studied area is a desert and very dry region, where rapid and extreme temperature changes within a short period of time are a prominent feature. Such a characteristic can also contribute to the observed differences between the model and observed data. The way the maximum and minimum temperature values are recorded in the manual synoptic stations and the hourly model simulations may not always align, leading to these discrepancies.

The almost uniform difference between the average and maximum temperatures simulated with observational data can indicate that some of these errors are systematic, which can be minimized by applying post-processing methods.

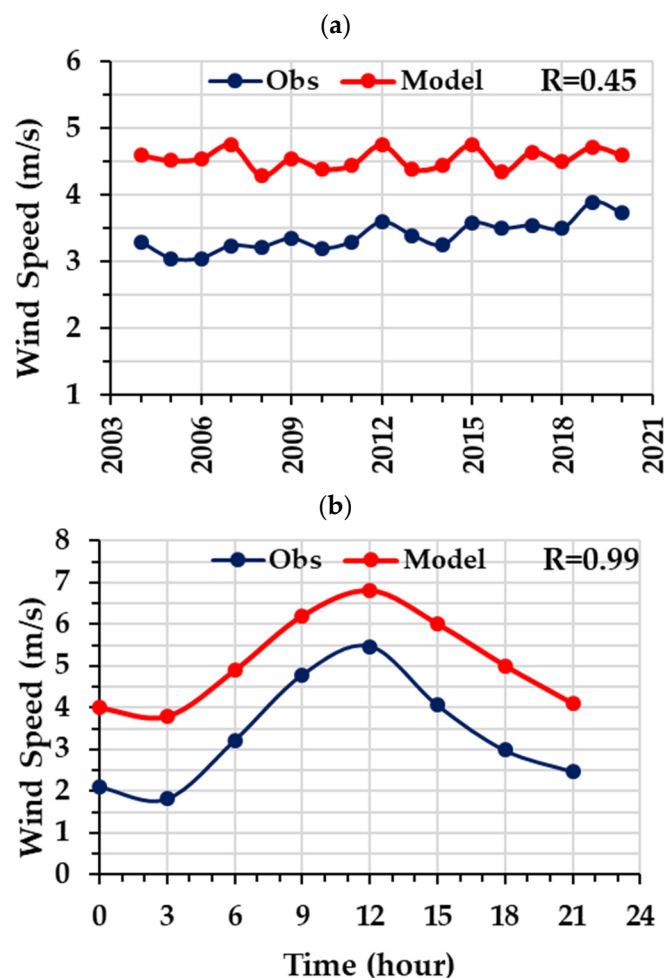
#### 4.2.2. WRF Model Simulations of Wind Speed and Wind Direction

Figure 6 shows the variation in annual mean 10 m wind speed (Figure 6a) and mean intraday variation in 10 m wind speed (Figure 6b) at Zahedan station in 2004–2020, obtained from the WRF model simulations and the measured data. Figure 6a shows that the model overestimated the annual value of the wind speed at the station during the whole study period. Since the correlation coefficient between the station data and the model outputs is moderate (0.45), it is obvious that the model did not simulate well the 10 m wind speed at Zahedan station. Figure 6b shows the mean diurnal variation in simulated and measured wind speed at Zahedan station. Like the previous simulation, the model overestimated 10 m wind speed; the highest difference is at 18 UTC (+2.02 m/s), and the lowest difference is at 12 UTC (+1.33 m/s). Although the correlation coefficient between the station wind data and simulation is very high (0.99), the result showed that the WRF model effectively simulated the 10 m wind speed changes in different hours of a day.

A comparison of observed wind speed changes with simulated data shows that the differences between them were almost the same during the day. However, the most significant errors occurred at the end of the day and early in the morning (Figure 6b). This suggests that the dry climate of the region, which experiences extreme cooling and heating during these time periods, is one of the main factors contributing to these differences.

The rapid and extreme temperature changes that occur in the desert and dry climate of the studied region, particularly towards the end of the day and the beginning of the night, appear to be a key driver of the discrepancies between the observed and simulated wind speed data. The model may not be accurately capturing the complex interactions between the temperature variations and wind patterns during these transitional periods, leading to the larger errors observed.

Addressing this issue may require further refinements to the model's representation of the region's unique microclimate and the associated wind dynamics, especially in the late afternoon and early morning hours when the temperature gradients are most pronounced. Applying targeted post-processing techniques or incorporating additional meteorological parameters into the model could help improve the simulation of wind speeds during these critical time periods.



**Figure 6.** (a) Variation in mean annual wind speed and (b) mean diurnal variation in the simulated 10 m wind speed (m/s) in UTC time at Zahedan station in 2004–2020.

Figure 7 shows the distributions of 10 m wind class frequency and the wind direction, as observed from the simulated and the observed data at Zahedan station in 2004–2020. The wind class frequency of the WRF model outputs (Figure 7a) is in good agreement with the station wind data (Figure 7b). The WRF model simulated the highest frequency of 10 m wind speed (56.3%), between 0.5 and 2.1 m/s, and the station data also show a maximum wind speed (56.2%) in the same range. The output of the WRF model effectively simulated the 10 m wind data in different ranges and distributions, but the percentage of 10 m wind data is different. Also, there is a huge discrepancy for the calm situation; the WRF model simulated the calm situation at 1% of total events, but the station data show the calm situation at 15.8% of the total in 2004–2020. The WRF model (Figure 7c) shows that the dominant wind direction was northwesterly and southwesterly, while the wind rose of the station observational data (Figure 7d) shows that wind direction was most probably north and northeasterly. The WRF model simulation revealed a northeast wind direction; thus, the simulated wind direction is distributed in a wider range of angles than the measured one.

The model excels in accurately simulating strong southwesterly and northerly winds exceeding 6 m/s. However, it encounters difficulties in representing weaker wind directions, especially westerlies, indicating a stronger proficiency in simulating systemic winds associated with dynamic low-pressure atmospheric systems rather than local wind patterns. The model's performance in simulating winds with speeds between 0.5 and 2 m/s is noteworthy.

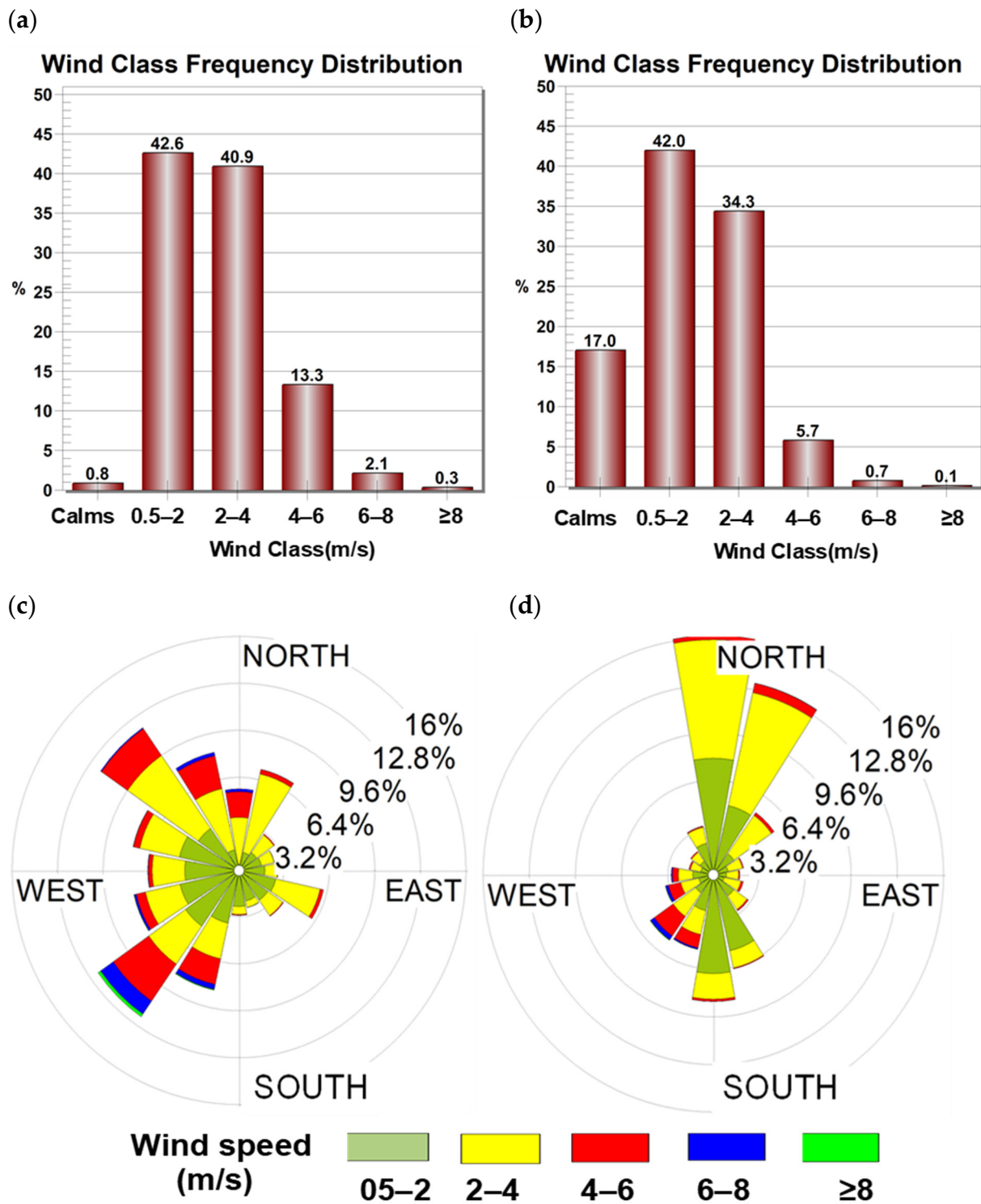
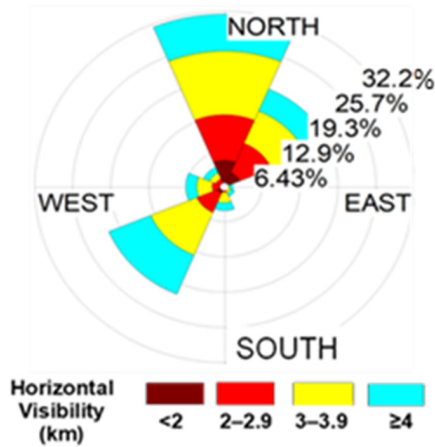


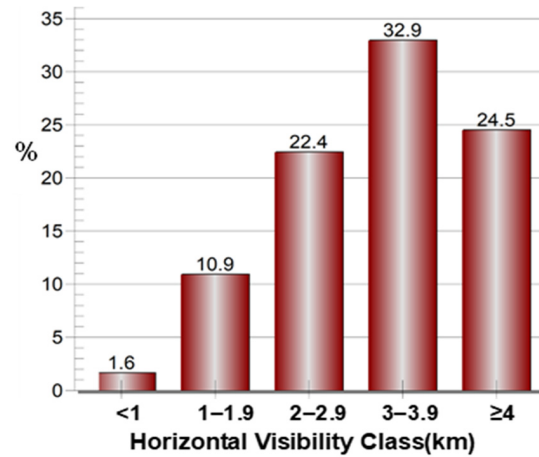
Figure 7. Wind rose by (a) WRF model simulation and (b) station observational data at Zahedan station in 2004–2020. Wind class frequency distribution by (c) WRF model simulation and (d) observed data at Zahedan station in 2004–2020.

Figure 8 presents the frequency distribution of horizontal visibility classes impacted by dust across various wind speeds and directions for all analyzed codes, specifically showcasing wind roses for code 06 (WW06) and code 07 (WW07). In Figure 8a, instead of displaying wind speed, the wind rose for the entire period from 2004 to 2021 is utilized to depict the values of reduced horizontal visibility due to dust, referred to as the dust rose.

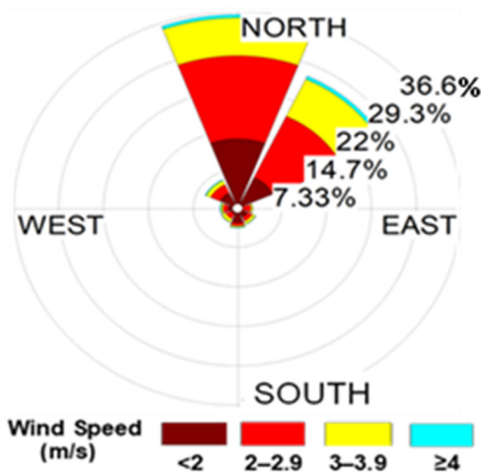
(a) WW06, 07, 30–35



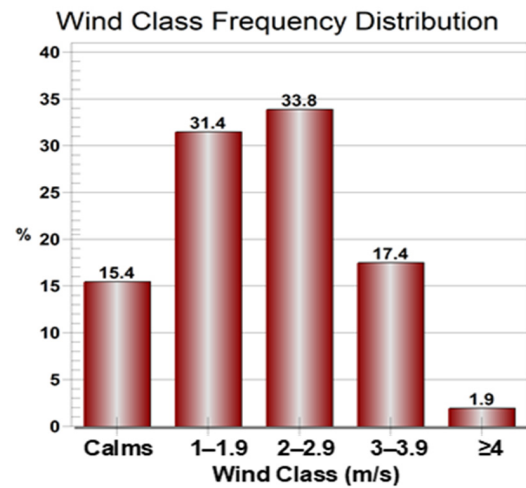
(b) WW06, 07, 30–35



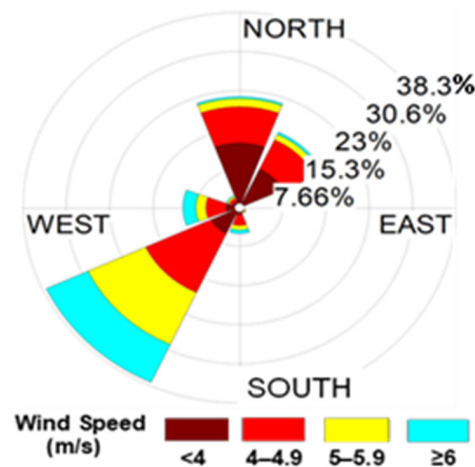
(c) WW06



(d) WW06



(e) WW07



(f) WW07

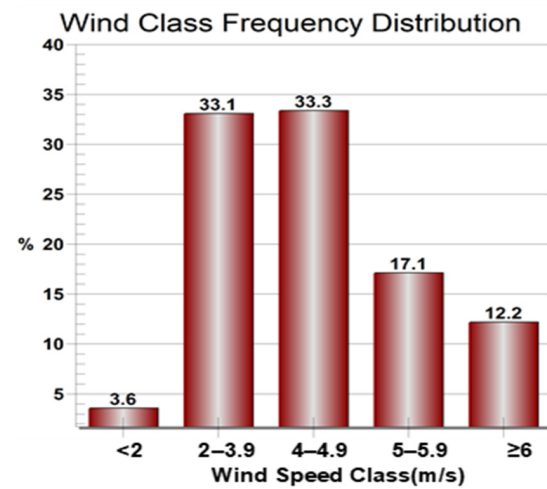


Figure 8. (a) Dust rose representation for codes 06, 07, and 30–35. (b) Frequency distribution of horizontal visibility classes for codes 06, 07, and 30–35. (c) Wind rose and (d) wind class frequency distribution for code 06. (e) Wind rose and (f) wind class frequency distribution for code 07. Based on observed data at Zahedan station from 2000 to 2021.

Within the total observations spanning from 2004 to 2021, amounting to 5748 cases, sand and dust storms were identified. Among these instances, 7.4% had incomplete data, 1.6% occurred during calm winds, 31.5% were linked to dust transported by northerly winds, 19.4% by northeast winds, 21.2% by southwesterly winds, 6.6% by westerly winds, and 10.3% by other wind directions (Figure 8a). Regarding horizontal visibility as an indicator of dust intensity, visibility less than 2 km signifies very strong to intense dust events, 2 km to 4 km indicates a moderate intensity, and above 4 km suggests weak intensity. The frequency distribution of reduced horizontal visibility due to dust reveals approximately 11.5% of very intense to intense dust events, and 55.3% of moderate-intensity and 24.5% of weak-intensity occurrences (Figure 8b).

Notably, there are three primary directional paths for dust entry into Zahedan city. To mitigate the population's exposure to resulting pollution, prioritizing dust management centers in these directions is recommended.

Figure 8c,d display the wind rose patterns and frequency distribution of each wind speed class associated with code 06. Around 36% of occurrences were linked to north winds, 27% to northeast winds, approximately 6% to northwest winds, and over 15% to calm wind conditions (Figure 8c).

Hence, one of the primary dust corridors from the north to the south into Zahedan is identified, suggesting the potential for mitigation by implementing control measures and managing dust centers in the vicinity of the desiccated Hamon Lake. Over 80% of these occurrences during the study period, wind speeds remained below 3 m/s, while winds equal to or exceeding 4 m/s were observed in less than 2% of the events (Figure 8d).

Analysis of the wind field associated with code 07 reveals that 22.8% of events were tied to north winds, 17.1% to northeast winds, 37.9% to southwest winds, and 10.4% to west winds (Figure 8e). Approximately 70% of cases were associated with wind speeds below 5 m/s, while 12.2% were associated with wind speeds equal to or greater than 6 m/s (Figure 8f).

## 5. Conclusions

In this study, the long-term (2000–2021) variation in dust event frequency at Zahedan station in the Sistan Basin of southeastern Iran, which is one of the important dust sources in Iran, was investigated. The dusty days were identified from dust-related codes 06, 07, 30 to 35, and 98 at Zahedan meteorological station in the Sistan Basin. The analysis showed that the annual number of dusty days was highest in 2008, with 157 days, and lowest in 2020, with 64 days. The highest seasonal dust event frequency was observed in the summer season, while the highest monthly dust event frequency occurred in July, in coincidence with the season of the Levar wind. The analysis of dust occurrences from 2004 to 2021 indicates a significant increase in dust persistence between 2004 and 2008, followed by a decrease from 2009 to 2021. This decline in dust persistence during the latter period is likely linked to shifts in atmospheric patterns, highlighting the dynamic nature of dust generation processes over the analyzed timeframe.

The analysis identified 5748 cases of sand and dust storms between 2004 and 2021, with significant contributions from northerly, northeast, and southwesterly wind directions. Notably, 31.5% of events were associated with northerly winds, 19.4% with northeast winds, and 21.2% with southwesterly winds. Prioritizing the management of dust sources aligned with these predominant wind directions can effectively reduce air pollution caused by dust storms.

The WRF simulations of air temperature revealed a systematic overestimation of the mean, maximum, and minimum air temperature compared to the station data, although the correlation coefficient values were high, especially for mean annual air temperature values reaching 0.8. Furthermore, the mean annual wind speed shows overestimation of WRF model wind data. The correlation coefficient between the model and the station data depicted a high correlation coefficient of 0.99 for mean intraday variations in air temperature and was low, at 0.45, for the case of mean annual air temperature variation.

The WRF model simulated well the highest 10 m wind class frequency distributions (42.6% of the total amount) distributed between 0.5 and 2 m/s, which is very close to the highest 10 m wind reported from the station (42.0% of total distributed between 0.5 and 2 m/s); however, the model simulated wind direction poorly. The WRF wind rose reconstructed wind direction in a wider range of values from southwesterly to northeasterly; however, the wind direction was predominately northerly from the station data.

The persistent discrepancies between simulated and observed quantities, particularly in temperature, reveal systematic errors within the model simulations that can be rectified through post-processing techniques. Notably, the inconsistencies in temperature and wind speed comparisons with observational data are more pronounced during late evening and early morning hours. These discrepancies may stem from extreme temperature fluctuations in desert areas during these periods, aspects that the model may inadequately address, leading to less accurate simulations at these specific times.

Since the wind speed and air temperature are two major meteorological factors for the simulations of dust emission from sources, as well as for dust transportation and propagation in the affected area, the discrepancies in the simulated and observed data of the parameters are crucial for under- or overestimation of model assessment of dust emission from hotspot areas.

**Author Contributions:** Conceptualization, N.H.H., A.R.S.A. and K.A.; methodology, N.H.H. and K.A.S.; software, N.H.H., A.R.S.A. and K.A.S.; validation, N.H.H., K.A.S. and A.R.S.A.; formal analysis, N.H.H., K.A.S., C.O. and A.R.S.A.; resources, N.H.H. and K.A.S.; data curation, N.H.H. and A.R.S.A.; writing—original draft preparation, N.H.H. and C.O.; writing—review and editing, A.R.S.A., K.A. and K.A.S.; visualization, N.H.H., K.A.S., A.R.S.A. and C.O. supervision, A.R.S.A. and K.A. All authors have read and agreed to the published version of the manuscript.

**Funding:** This research received no external funding.

**Institutional Review Board Statement:** Not applicable.

**Informed Consent Statement:** Not applicable.

**Data Availability Statement:** The data presented in this study are available on request from the corresponding author. The data are not publicly available due to restriction policy of ASMERC.

**Acknowledgments:** The authors are greatly thankful to the Iranian meteorological organization (IRIMO) and atmospheric science and meteorology research center (ASMERC) for WRF model running and dust-related codes.

**Conflicts of Interest:** Nasim Hossein Hamzeh is an employee of the Air and Climate Technology Company (ACTC). The paper reflects the views of the scientists and not the company. The authors declare no conflicts of interest.

## Abbreviations

ACM2	Asymmetric Convective Model Version 2
DD	Dusty day
ECMWF	European Centre for Medium-Range Weather Forecasts
ERA5	ECMWF Reanalysis v5
MYJ	Mellor, Yamada, and Janjić
MYNN2.5	Mellor–Yamada–Nakanishi–Niino
PBL	Planetary Boundary Layer
PM10	Particulate matter with an aerodynamic diameter of less than 10 micrometers ( $\mu\text{m}$ )
RRTM	Rapid Radiative Transfer Model
SDS	sand and dust storm
QNSE	Quasi-Normal Scale Elimination
WW	present Weather
YSU	Yonsei University

## References

1. Griffin, D.W.; Kellogg, C.A. Dust storms and their impact on ocean and human health: Dust in earth's atmosphere. *Ecohealth* **2004**, *1*, 284–295. [[CrossRef](#)]
2. Sissakian, V.K.; Al-Ansari, N.; Knutsson, S. Sand and dust storm events in Iraq. *J. Nat. Sci.* **2013**, *5*, 1084–1094. [[CrossRef](#)]
3. Kok, J.F.; Adebisi, A.A.; Albani, S.; Balkanski, Y.; Checa-Garcia, R.; Chin, M.; Colarco, P.R.; Hamilton, D.S.; Huang, Y.; Ito, A.; et al. Contribution of the world's main dust source regions to the global cycle of desert dust. *Atmos. Chem. Phys.* **2021**, *21*, 8169–8193. [[CrossRef](#)]
4. Darvishi Bolorani, A.; Papi, R.; Soleimani, M.; Karami, L.; Amiri, F.; Samany, N.N. Water bodies changes in Tigris and Euphrates basin has impacted dust storms phenomena. *Aeolian Res.* **2021**, *50*, 100698. [[CrossRef](#)]
5. Hamzeh, N.H.; Shukurov, K.; Mohammadpour, K.; Kaskaoutis, D.G.; Abadi, A.R.S.; Shahabi, H. A comprehensive investigation of the causes of drying and increasing saline dust in the Urmia Lake, northwest Iran, via ground and satellite observations, synoptic analysis and machine learning models. *Ecol. Inform.* **2023**, *78*, 102355. [[CrossRef](#)]
6. Hamzeh, N.H.; Abadi, A.R.S.; Shukurov, K.A.; Mhawish, A.; Alam, K.; Opp, C.; Meteorology, K.N.C.F.; Marburg, G.P.-U. Simulation and synoptic investigation of a severe dust storm originated from the Urmia Lake in the Middle East. *Atmosfera* **2024**, *38*, 531–555. [[CrossRef](#)]
7. Abadi, A.R.S.; Hamzeh, N.H.; Shukurov, K.; Opp, C.; Dumka, U.C. Long-term investigation of aerosols in the Urmia Lake region in the Middle East by ground-based and satellite data in 2000–2021. *Remote Sens.* **2022**, *14*, 3827. [[CrossRef](#)]
8. Hamzeh, N.H.; Abadi, A.R.S.; Kaskaoutis, D.G.; Mirzaei, E.; Shukurov, K.A.; Sotiropoulou, R.-E.P.; Tagaris, E. The Importance of Wind Simulations over Dried Lake Beds for Dust Emissions in the Middle East. *Atmosphere* **2023**, *15*, 24. [[CrossRef](#)]
9. Hamzeh, N.H.; Kaskaoutis, D.G.; Rashki, A.; Mohammadpour, K. Long-term variability of dust events in southwestern Iran and its relationship with the drought. *Atmosphere* **2021**, *12*, 1350. [[CrossRef](#)]
10. Rashki, A.; Middleton, N.J.; Goudie, A.S. Dust storms in Iran—Distribution, causes, frequencies and impacts. *Aeolian Res.* **2020**, *48*, 100655. [[CrossRef](#)]
11. Maleki, S.; Miri, A.; Rahdari, V.; Dragovich, D. A method to select sites for sand and dust storm source mitigation: Case study in the Sistan region of southeast Iran. *J. Environ. Plan. Manag.* **2021**, *64*, 2192–2213. [[CrossRef](#)]
12. Lababpour, A. The response of dust emission sources to climate change: Current and future simulation for southwest of Iran. *Sci. Total Environ.* **2020**, *714*, 136821. [[CrossRef](#)] [[PubMed](#)]
13. Cao, H.; Liu, J.; Wang, G.; Yang, G.; Luo, L. Identification of sand and dust storm source areas in Iran. *J. Arid. Land* **2015**, *7*, 567–578. [[CrossRef](#)]
14. Adib, A.; Oulapour, M.; Chatroze, A. Effects of wind velocity and soil characteristics on dust storm generation in Hawr-al-Azim Wetland, Southwest Iran. *Casp. J. Environ. Sci.* **2018**, *16*, 333–347.
15. Broomandi, P.; Dabir, B.; Bonakdarpour, B.; Rashidi, Y. Identification of dust storm origin in South–West of Iran. *J. Environ. Health Sci. Eng.* **2017**, *15*, 16. [[CrossRef](#)] [[PubMed](#)]
16. Karami, S.; Hamzeh, N.H.; Kaskaoutis, D.G.; Rashki, A.; Alam, K.; Ranjbar, A. Numerical simulations of dust storms originated from dried lakes in central and southwest Asia: The case of Aral Sea and Sistan Basin. *Aeolian Res.* **2021**, *50*, 100679. [[CrossRef](#)]
17. Rashki, A.; Kaskaoutis, D.G.; Rautenbach, C.J.D.; Eriksson, P.G.; Qiang, M.; Gupta, P. Dust storms and their horizontal dust loading in the Sistan region, Iran. *Aeolian Res.* **2012**, *5*, 51–62. [[CrossRef](#)]
18. Zucca, C.; Middleton, N.; Kang, U.; Liniger, H. Shrinking water bodies as hotspots of sand and dust storms: The role of land degradation and sustainable soil and water management. *Catena* **2021**, *207*, 105669. [[CrossRef](#)]
19. Beyranvand, A.; Azizi, G.; Alizadeh, O.; Bolorani, A.D. Dust in Western Iran: The emergence of new sources in response to shrinking water bodies. *Sci. Rep.* **2023**, *13*, 16158. [[CrossRef](#)]
20. Rashki, A.; Kaskaoutis, D.; Goudie, A.; Kahn, R. Dryness of ephemeral lakes and consequences for dust activity: The case of the Hamoun drainage basin, southeastern Iran. *Sci. Total Environ.* **2013**, *463–464*, 552–564. [[CrossRef](#)]
21. Rashki, A.; Kaskaoutis, D.; Francois, P.; Kosmopoulos, P.; Legrand, M. Dust-storm dynamics over Sistan region, Iran: Seasonality, transport characteristics and affected areas. *Aeolian Res.* **2015**, *16*, 35–48. [[CrossRef](#)]
22. Hamidianpour, M.; Jahanshahi, S.M.A.; Kaskaoutis, D.G.; Rashki, A.; Nastos, P.G. Climatology of the Sistan Levant wind: Atmospheric dynamics driving its onset, duration and withdrawal. *Atmos. Res.* **2021**, *260*, 105711. [[CrossRef](#)]
23. Alizadeh, O.; Abniki, M.; Babaei, M.; Irannejad, P. Climatology and the dynamic mechanism of the Levant wind and dust events in eastern Iran. *Int. J. Clim.* **2022**, *42*, 9288–9303. [[CrossRef](#)]
24. An, L.; Che, H.; Xue, M.; Zhang, T.; Wang, H.; Wang, Y.; Zhou, C.; Zhao, H.; Gui, K.; Zheng, Y.; et al. Temporal and spatial variations in sand and dust storm events in East Asia from 2007 to 2016: Relationships with surface conditions and climate change. *Sci. Total Environ.* **2018**, *633*, 452–462. [[CrossRef](#)] [[PubMed](#)]
25. Alizadeh-Choozari, O.; Zavar-Reza, P.; Sturman, A. The “wind of 120 days” and dust storm activity over the Sistan Basin. *Atmos. Res.* **2014**, *143*, 328–341. [[CrossRef](#)]
26. Csavina, J.; Field, J.; Félix, O.; Corral-Avitia, A.Y.; Sáez, A.E.; Betterton, E.A. Effect of wind speed and relative humidity on atmospheric dust concentrations in semi-arid climates. *Sci. Total Environ.* **2014**, *487*, 82–90. [[CrossRef](#)] [[PubMed](#)]
27. Dar, M.A.; Ahmed, R.; Latif, M.; Azam, M. Climatology of dust storm frequency and its association with temperature and precipitation patterns over Pakistan. *Nat. Hazards* **2022**, *110*, 655–677. [[CrossRef](#)]

28. Karami, S.; Hamzeh, N.H.; Abadi, A.R.S.; Madhavan, B.L. Investigation of a severe frontal dust storm over the Persian Gulf in February 2020 by CAMS model. *Arab. J. Geosci.* **2021**, *14*, 2041. [[CrossRef](#)]
29. Karami, S.; Hamzeh, N.H.; Noori, F.; Ranjbar, A. Investigation of dust storms in Ilam and the performance analysis of simulation of 6 numerical prediction models at a severe dust storm in west of Iran. *J. Air Pollut. Health* **2019**, *4*, 133–146. [[CrossRef](#)]
30. Liu, X.D.; Yin, Z.Y.; Zhang, X.-Y.; Yang, X.C. Analyses of the spring dust storm frequency of northern China in relation to antecedent and concurrent wind, precipitation, vegetation, and soil moisture conditions. *J. Geophys. Res. Space Phys.* **2004**, *109*, D16210. [[CrossRef](#)]
31. Kim, D.; Chin, M.; Remer, L.A.; Diehl, T.; Bian, H.; Yu, H.; Brown, M.E.; Stockwell, W.R. Role of surface wind and vegetation cover in multi-decadal variations of dust emission in the Sahara and Sahel. *Atmos. Environ.* **2016**, *148*, 282–296. [[CrossRef](#)]
32. Hamzeh, N.H.; Karami, S.; Kaskaoutis, D.G.; Tegen, I.; Moradi, M.; Opp, C. Atmospheric dynamics and numerical simulations of six frontal dust storms in the Middle East region. *Atmosphere* **2021**, *12*, 125. [[CrossRef](#)]
33. Xu, J.; Hou, S.; Qin, D.; Kang, S.; Ren, J.; Ming, J. Dust storm activity over the Tibetan Plateau recorded by a shallow ice core from the north slope of Mt. Qomolangma (Everest), Tibet-Himal region. *Geophys. Res. Lett.* **2007**, *34*, L17504. [[CrossRef](#)]
34. Zhai, L.; Sun, Z.; Li, Z.; Yin, X.; Xiong, Y.; Wu, J.; Li, E.; Kou, X. Dynamic effects of topography on dust particles in the Beijing region of China. *Atmos. Environ.* **2019**, *213*, 413–423. [[CrossRef](#)]
35. Saadatabadi, A.R.; Hamzeh, N.H.; Kaskaoutis, D.G.; Ghasabi, Z.; Penchah, M.M.; Sotiropoulou, R.-E.P.; Habibi, M. Optimization and evaluation of the Weather Research and Forecasting (WRF) model for wind energy resource assessment and mapping in Iran. *Appl. Sci.* **2024**, *14*, 3304. [[CrossRef](#)]
36. Yang, B.; Bräuning, A.; Zhang, Z.; Dong, Z.; Esper, J. Dust storm frequency and its relation to climate changes in Northern China during the past 1000 years. *Atmos. Environ.* **2007**, *41*, 9288–9299. [[CrossRef](#)]
37. Goossens, D.; Offer, Z.Y. Wind tunnel and field calibration of six aeolian dust samplers. *Atmos. Environ.* **2000**, *34*, 1043–1057. [[CrossRef](#)]
38. Preston, C.A.; Neuman, C.M.; Boulton, J.W. A wind tunnel and field evaluation of various dust suppressants. *J. Air Waste Manag. Assoc.* **2020**, *70*, 915–931. [[CrossRef](#)]
39. Zhang, J.; Shao, Y.; Huang, N. Measurements of dust deposition velocity in a wind-tunnel experiment. *Atmos. Meas. Technol.* **2014**, *14*, 8869–8882. [[CrossRef](#)]
40. Shannak, B.; Corsmeier, U.; Kottmeier, C.; Al-Azab, T. Wind tunnel study of twelve dust samples by large particle size. *Atmos. Environ.* **2014**, *98*, 442–453. [[CrossRef](#)]
41. Draxler, R.R.; Hess, G.D. An overview of the HYSPLIT\_4 modelling system for trajectories. *Aust. Meteorol. Mag.* **1998**, *47*, 295–308.
42. Escudero, M.; Stein, A.; Draxler, R.R.; Querol, X.; Alastuey, A.; Castillo, S.; Avila, A. Determination of the contribution of northern Africa dust source areas to PM<sub>10</sub> concentrations over the central Iberian Peninsula using the Hybrid Single-Particle Lagrangian Integrated Trajectory model (HYSPLIT) model. *J. Geophys. Res. Atmos.* **2006**, *111*, D06210. [[CrossRef](#)]
43. McGowan, H.; Clark, A. Identification of dust transport pathways from Lake Eyre, Australia using Hysplit. *Atmos. Environ.* **2008**, *42*, 6915–6925. [[CrossRef](#)]
44. Kurosaki, Y.; Mikami, M. Threshold wind speed for dust emission in east Asia and its seasonal variations. *J. Geophys. Res. Atmos.* **2007**, *112*, D17202. [[CrossRef](#)]
45. Webb, N.P.; Strong, C.L. Soil erodibility dynamics and its representation for wind erosion and dust emission models. *Aeolian Res.* **2011**, *3*, 165–179. [[CrossRef](#)]
46. Gillette, D.A.; Passi, R. Modeling dust emission caused by wind erosion. *J. Geophys. Res. Atmos.* **1988**, *93*, 14233–14242. [[CrossRef](#)]
47. Tian, M.; Gao, J.; Zhang, L.; Zhang, H.; Feng, C.; Jia, X. Effects of dust emissions from wind erosion of soil on ambient air quality. *Atmos. Pollut. Res.* **2021**, *12*, 101108. [[CrossRef](#)]
48. Liu, M.; Westphal, D.L.; Holt, T.R.; Xu, Q. Numerical Simulation of a Low-Level Jet over Complex Terrain in Southern Iran. *Mon. Weather Rev.* **2000**, *128*, 1309–1327. [[CrossRef](#)]
49. Parno, R.; Meshkatee, A.-H.; Hassan, E.M.; Hamzeh, N.H.; Ooi, M.C.G.; Habibi, M. Investigating the Role of the Low-Level Jet in Two Winters Severe Dust Rising in Southwest Iran. *Atmosphere* **2024**, *15*, 400. [[CrossRef](#)]
50. Abadi, A.R.S.; Hamzeh, N.H.; Ooi, M.C.G.; Kong, S.S.-K.; Opp, C. Investigation of two severe shamal dust storms and the highest dust frequencies in the South and Southwest of Iran. *Atmosphere* **2022**, *13*, 1990. [[CrossRef](#)]
51. Alizadeh-Choozari, O.; Ghafarian, P.; Owlad, E. Temporal variations in the frequency and concentration of dust events over Iran based on surface observations. *Int. J. Climatol.* **2016**, *36*, 2050–2062. [[CrossRef](#)]
52. Asghari, M.; Meshkatee, A.; Abadi, A.R.S.; Moradi, M. Investigation of Atmospheric Pattern and Simulation of the Frontal Sandstorm Emission over Eastern and Southeastern Iran (case study 23 & 24 April 2019). *Pollution* **2021**, *7*, 73–85. [[CrossRef](#)]
53. Rashki, A.; Kaskaoutis, D.G.; Sepehr, A. Statistical evaluation of the dust events at selected stations in Southwest Asia: From the Caspian Sea to the Arabian Sea. *Catena* **2018**, *165*, 590–603. [[CrossRef](#)]
54. Behrooz, R.D.; Mohammadpour, K.; Broomandi, P.; Kosmopoulos, P.G.; Gholami, H.; Kaskaoutis, D.G. Long-term (2012–2020) PM<sub>10</sub> concentrations and increasing trends in the Sistan Basin: The role of Levar wind and synoptic meteorology. *Atmos. Pollut. Res.* **2022**, *13*, 101460. [[CrossRef](#)]
55. Rashki, A.; Kaskaoutis, D.G.; Mofidi, A.; Minvielle, F.; Chiapello, I.; Legrand, M.; Dumka, U.C.; Francois, P. Effects of Monsoon, Shamal and Levar winds on dust accumulation over the Arabian Sea during summer—The July 2016 case. *Aeolian Res.* **2018**, *36*, 27–44. [[CrossRef](#)]



56. Choobari, O.A.; Zawar-Reza, P.; Sturman, A. The global distribution of mineral dust and its impacts on the climate system: A review. *Atmos. Res.* **2014**, *138*, 152–165. [[CrossRef](#)]
57. Miri, A.; Ahmadi, H.; Ekhtesasi, M.R.; Panjehkeh, N.; Ghanbari, A. Environmental and socio-economic impacts of dust storms in Sistan Region, Iran. *Int. J. Environ. Stud.* **2009**, *66*, 343–355. [[CrossRef](#)]
58. Rashki, A.; Rautenbach, C.J.D.; Eriksson, P.G.; Kaskaoutis, D.G.; Gupta, P. Temporal changes of particulate concentration in the ambient air over the city of Zahedan, Iran. *Air Qual. Atmos. Health* **2011**, *6*, 123–135. [[CrossRef](#)]
59. Hersbach, H.; De Rosnay, P.; Bell, B.; Schepers, D.; Simmons, A.; Soci, C.; Abdalla, S.; Alonso-Balmaseda, M.; Balsamo, G.; Bechtold, P.; et al. *Operational Global Reanalysis: Progress, Future Directions and Synergies with NWP*; Elsevier: Amsterdam, The Netherlands, 2018.
60. Hersbach, H. ERA5 reanalysis is in production. *ECMWF Newsl.* **2016**, *147*, 5.
61. Sathe, Y.; Kulkarni, S.; Gupta, P.; Kaginalkar, A.; Islam, S.; Gargava, P. Application of Moderate Resolution Imaging Spectroradiometer (MODIS) Aerosol Optical Depth (AOD) and Weather Research Forecasting (WRF) model meteorological data for assessment of fine particulate matter (PM<sub>2.5</sub>) over India. *Atmos. Pollut. Res.* **2018**, *10*, 418–434. [[CrossRef](#)]
62. Najafpour, N.; Afshin, H.; Firoozabadi, B. Sensitivity study and comparative evaluation of WRF-Chem over Iran: Available and embedded dust emission schemes. *Atmos. Pollut. Res.* **2023**, *14*, 101930. [[CrossRef](#)]
63. Ali, G.; Bao, Y.; Asmerom, B.; Ullah, W.; Ullah, S.; Arshad, M. Assessment of the simulated aerosol optical properties and regional meteorology using WRF-Chem model. *Arab. J. Geosci.* **2021**, *14*, 1871. [[CrossRef](#)]
64. Xi, X. Revisiting the recent dust trends and climate drivers using horizontal visibility and present weather observations. *J. Geophys. Res. Atmos.* **2021**, *126*, e2021JD034687. [[CrossRef](#)]
65. Yu, Y.; Notaro, M.; Liu, Z.; Wang, F.; Alkolibi, F.; Fadda, E.; Bakhrjy, F. Climatic Controls on the Interannual to Decadal Variability in Saudi Arabian Dust Activity: Toward the Development of a Seasonal Dust Prediction Model: Saudi Arabian Dust Prediction. *J. Geophys. Res.* **2015**, *120*, 1739–1758. [[CrossRef](#)]
66. Notaro, M.; Yu, Y.; Kalashnikova, O.V. Regime shift in Arabian dust activity, triggered by persistent Fertile Crescent drought. *J. Geophys. Res. Atmos.* **2015**, *120*, 110–229. [[CrossRef](#)]
67. Klingmüller, K.; Pozzer, A.; Metzger, S.; Stenchikov, G.L.; Lelieveld, J. Aerosol optical depth trend over the Middle East. *Atmos. Chem. Phys. Discuss.* **2016**, *16*, 5063–5073. [[CrossRef](#)]
68. Yousefi, R.; Wang, F.; Ge, Q.; Lelieveld, J.; Shaheen, A. Aerosol Trends during the Dusty Season over Iran. *Remote Sens.* **2021**, *13*, 1045. [[CrossRef](#)]
69. Al-Dousari, A.M.; Al-Awadhi, J. Dust fallout in northern Kuwait, major sources and characteristics. *Kuwait J. Sci.* **2012**, *39*, 171–187.
70. Penchah, M.M.; Malakooti, H.; Satkin, M. Evaluation of planetary boundary layer simulations for wind resource study in east of Iran. *Renew. Energy* **2017**, *111*, 1–10. [[CrossRef](#)]
71. Al Ameri, I.D.S.; Briant, R.M.; Engels, S. Drought severity and increased dust storm frequency in the Middle East: A case study from the Tigris–Euphrates alluvial plain, central Iraq. *Weather* **2019**, *74*, 416–426. [[CrossRef](#)]
72. Lin, Y.L.; Farley, R.D.; Orville, H.D. Bulk parameterization of the snow field in a cloud model. *J. Appl. Meteorol. Climatol.* **1983**, *22*, 1065–1092. [[CrossRef](#)]
73. Mlawer, E.J.; Taubman, S.J.; Brown, P.D.; Iacono, M.J.; Clough, S.A. Radiative transfer for inhomogeneous atmospheres: RRTM, a validated correlated-k model for the longwave. *J. Geophys. Res. Atmos.* **1997**, *102*, 16663–16682. [[CrossRef](#)]
74. Dudhia, J. Numerical study of convection observed during the winter monsoon experiment using a mesoscale two-dimensional model. *J. Atmos. Sci.* **1989**, *46*, 3077–3107. [[CrossRef](#)]
75. Niu, G.Y.; Yang, Z.L.; Mitchell, K.E.; Chen, F.; Ek, M.B.; Barlage, M.; Kumar, A.; Manning, K.; Niyogi, D.; Rosero, E.; et al. The community Noah land surface model with multiparameterization options (Noah-MP): 1. Model description and evaluation with local-scale measurements. *J. Geophys. Res. Atmos.* **2011**, *116*, D12109.
76. Hu, X.M.; Nielsen-Gammon, J.W.; Zhang, F. Evaluation of three planetary boundary layer schemes in the WRF model. *J. Appl. Meteorol. Climatol.* **2010**, *49*, 1831–1844.
77. Parolari, A.J.; Li, D.; Bou-Zeid, E.; Katul, G.G.; Assouline, S. Climate, not conflict, explains extreme Middle East dust storm. *Environ. Res. Lett.* **2016**, *11*, 114013. [[CrossRef](#)]
78. Mousavi, H.; Panahi, D.M.; Kalantari, Z.; Mousavi, H.; Panahi, D.M.; Kalantari, Z. Dust and climate interactions in the Middle East: Spatio-temporal analysis of aerosol optical depth and climatic variables. *Sci. Total Environ.* **2024**, *927*, 172176. [[CrossRef](#)] [[PubMed](#)]
79. Javadian, M.; Behrangi, A.; Sorooshian, A. Impact of drought on dust storms: Case study over Southwest Iran. *Environ. Res. Lett.* **2019**, *14*, 124029. [[CrossRef](#)]
80. Middleton, N.J. Desert dust hazards: A global review. *Aeolian Res.* **2017**, *24*, 53–63. [[CrossRef](#)]
81. Li, J.; Garshick, E.; Al-Hemoud, A.; Huang, S.; Koutrakis, P. Impacts of meteorology and vegetation on surface dust concentrations in Middle Eastern countries. *Sci. Total Environ.* **2020**, *712*, 136597. [[CrossRef](#)]
82. Shukurov, K.A.; Simonenkov, D.V.; Nevzorov, A.V.; Rashki, A.; Hamzeh, N.H.; Abdullaev, S.F.; Shukurova, L.M.; Chkhetiani, O.G. CALIOP-Based Evaluation of Dust Emissions and Long-Range Transport of the Dust from the Aral–Caspian Arid Region by 3D-Source Potential Impact (3D-SPI) Method. *Remote Sens.* **2023**, *15*, 2819. [[CrossRef](#)]

83. Najafi, M.S.; Khoshakhlagh, F.; Zamanzadeh, S.M.; Shirazi, M.H.; Samadi, M.; Hajikhani, S. Characteristics of TSP Loads during the Middle East Springtime Dust Storm (MESDS) in Western Iran. *Arab. J. Geosci.* **2013**, *7*, 5367–5381. [[CrossRef](#)]
84. Khoshakhlagh, F.; Najafi, M.S.; Samadi, M. An analysis on synoptic patterns of springtime dust occurrence in West of Iran. *Phys. Geogr. Res.* **2012**, *44*, 99–124.
85. Baghbanan, P.; Ghavidel, Y.; Farajzadeh, M. Spatial analysis of spring dust storms hazard in Iran. *Theor. Appl. Clim.* **2020**, *139*, 1447–1457. [[CrossRef](#)]
86. Kamal, A.; Lin, Z.; Wu, C. Decadal change of spring dust activity in western Iran and its mechanism. *Front. Environ. Sci.* **2022**, *10*, 983048. [[CrossRef](#)]
87. Ghasem, A.; Shamsipour, A.; Miri, M.; Safarrad, T. Synoptic and remote sensing analysis of dust events in southwestern Iran. *Nat. Hazards* **2012**, *64*, 1625–1638. [[CrossRef](#)]
88. Broomandi, P.; Karaca, F.; Guney, M.; Fathian, A.; Geng, X.; Kim, J.R. Destinations frequently impacted by dust storms originating from southwest Iran. *Atmos. Res.* **2021**, *248*, 105264. [[CrossRef](#)]

**Disclaimer/Publisher’s Note:** The statements, opinions and data contained in all publications are solely those of the individual author(s) and contributor(s) and not of MDPI and/or the editor(s). MDPI and/or the editor(s) disclaim responsibility for any injury to people or property resulting from any ideas, methods, instructions or products referred to in the content.